Trapped microplastics within vertical redeposited sediment: Experimental study simulating lake and channeled river systems during resuspension events

Mel Constant, Claire Alary, Lisa Weiss, Alix Constant, Gabriel Billon

Trapped microplastics within vertical redeposited sediment: Experimental study simulating lake and channeled river systems during resuspension events

Mel Constant[1*], Claire Alary[1], Lisa Weiss[2,3], Alix Constant[1] and Gabriel Billon[4]

[1]Univ. Lille, Institut Mines-Télécom, Univ. Artois, Junia, ULR 4515 - LGCgE, Laboratoire de Génie Civil et géo-Environnement, F-59000 Lille, France

[2] Université de Toulouse III, CNES, CNRS, IRD, UMR 5566 – LEGOS, Laboratoire d'Etudes en Géophysique et Océanographie Spatiales, F-31400 Toulouse, France

[3]Université de Bretagne Occidentale, IUEM, CNRS, IRD, Ifremer, UMR 6523 - LOPS, Laboratoire d'Océanographie Physique et Spatiale, F-29280 Plouzané, France

[4]Univ. Lille, CNRS, UMR 8516 - LASIRE, Laboratoire Avancé de Spectroscopie pour les Interactions, la Réactivité et l'Environnement, F-59000 Lille, France

*corresponding author: mel.constant@lilo.org

Keywords: Microplastics, river sediments, low-velocity flow, deposition, settling velocity.

Abstract

Plastic waste and its fragments (microplastics; <5 mm) have been observed in almost all types of environments. However, the mechanisms underlying the flow and transport processes of plastics are unknown. This is particularly valid for river sediments, where complex interactions occur between particles and influence their vertical and horizontal distribution patterns. In this study, we investigated the vertical redistribution of 14 pristine microplastics (MPs) with different densities, sizes, and shapes within disturbed sediment without lateral transport (i.e., low-velocity flow). MPs were spiked into sediments (height: 8 cm) in a column with a height of 1 m (diameter: 6 cm) filled to the top with water. The sediment was perturbed by turning the column upside-down to simulate remobilization and the subsequent deposition of sediment. After the complete sedimentation of the particles, the water column was filtered and the sediment was cut into vertical sections. MPs were then extracted from the sediment using sieves and a density separation method, and were counted under a stereomicroscope. Low-density polymers were mainly recovered in the water column and at the surface of the sediment, whereas high-density polymers were found within all sediment sections. The vertical distribution of high-density polymers changes primarily with the sediment grain size. The distribution of each polymer type changes depending on the size and/or shape of the particles with complex interactions. The observed distributions were compared with the expected distributions based only on the vertical velocity formulas. Overall, the formulas used did not explain the sedimentation of a portion of low-density polymers and predicted a lower distribution in the sediment than those observed in the experiment. In conclusion, this study highlights the importance of considering MPs as multi-dimensional particles and provides clues to understand their fate in low-velocity flow systems, considering that they undergo scavenging in sediments.

1. Introduction

Attention to microplastics (MPs) and their economic, social, and environmental issues has increased over the last few decades (Horton, 2021). MPs are found everywhere, from mountains to central open oceans, and are transported by winds, adrift in water bodies, deposited or trapped in sediment, and captured inside organisms (*e.g.*, Allen et al., 2019; Constant et al., 2021a; Miller et al., 2017; Santos et al., 2021). Plastics have a slow degradation rate under most environmental conditions and can therefore persist for long periods of time (Andrady, 2015). Moreover, plastic materials can contain or adsorb contaminants (Rochman, 2015). MPs are of particular concern because both the probability of entering the bodies of organisms (through ingestion or inhalation) and the reaction/adsorption surface increase with decreasing size (GESAMP, 2015).

The majority of marine litter is known to have a land-based origin (UNEP and GRID-Arendal, 2016) and rivers are considered as the main conveyors transporting MPs from terrestrial to marine ecosystems (Lebreton and Andrady, 2019). Observations also suggest that rivers can act as a sink for MPs trapped in sediment (Constant et al., 2021a), as is evident for other pollutants, including trace metals and organic substances. MPs can accumulate or be remobilized at higher flow velocities. The quantitative and temporal extent of this sequestration is poorly understood, but it is of paramount importance, both for the exposure of benthic organisms and for the global budget of MPs. Despite an increasing number of studies to identify and quantify MPs in aquatic environments, their sources, transport, and fate remain unclear (Petersen and Hubbart, 2021; Rochman, 2018; Zhang et al., 2020; Constant et al., 2017; Weiss et al., 2021). This is particularly true for the behavior of MPs in freshwater, including sediments (Waldschläger et al., 2022; He et al., 2021). This lack of understanding restricts our ability to properly estimate and understand the distribution of MPs in rivers and their export to the oceans (Waldschläger and Schüttrumpf, 2019a).

In the water column, the movement of particles depends on their properties, hydrodynamics, and interactions with other particles (Waldschläger and Schüttrumpf, 2019b). Sediment and/or contaminant transport models generally integrate the density and size as parameters of particle

properties (Nizzetto et al., 2016). The first theoretical assessment of MP transport assumed that the behavior of MPs is similar to that of sediments (Kooi et al., 2018). However, MPs are characterized by a broad range of densities, sizes, and shapes (Rochman et al., 2019). Therefore, plastics and sediments may behave differently (Waldschläger and Schüttrumpf, 2019). In particular, sediment shapes range from nearly spherical (e.g., mature siliciclastic sediment) to nearly flat (e.g., muscovite and biotite), and MPs mainly comprise fibers (elongated and thin cylinders; Constant et al., 2021a). Understanding the similarities and differences between the behaviors of MPs and sediment, as well as their interactions, is of particular interest for the accurate estimation of MP deposition in river sediments.

This study aims to better understand the distribution of several MP types in sediment that were recently deposited after perturbation under low-velocity flow conditions (e.g., barge traffic in canals or dredging) through column experiments and theoretical approaches. Low-velocity flows are common in lakes and anthropic waterways such as canals, which result in favorable conditions for the deposition of particles. The objectives of our study were to: (1) observe the influence of MP and sediment parameters on the redistribution of MPs; (2) predict the distribution of MPs based only on vertical velocity formulas using MP and sediment features (size, shape, and density); and (3) compare the experimental and theoretical data to identify the key parameters explaining the differences between observations and a simple theoretical sedimentation situation.

Several field studies has investigated the link between sediment grain size and MP (e.g. Constant et al., 2021a; Corcoran et al., 2020; Dhivert et al., 2022; Vermaire et al., 2017). However, experiments on the sedimentation of particles and MPs have been carried out separately, while laboratory tests are crucial for understanding this relationship, highly complex in the nature. This study investigates them together. The results are expected to help future studies to better estimate the complex sedimentation of MPs, improve global budgets, and predict future trends. Notably, we demonstrate the extent to which sediments can be a sink for the densest MPs, redistributed within the sediment column, and also how sediments can be a source of MPs when they are resuspended. These experiments and

89 simulations will integrate in the future the lateral transport of particles to improve models and to study
90 the export of these pollutants from terrestrial to marine environments.

2. Materials and methods

2.1. Column experiments: observed distribution

2.1.1. Spiked pristine microplastics and sediments

In each experiment, we used a mixture of low- and high-density polymers with different sizes and shapes (Table 1 and Fig. A.1). We used polyethylene (PE; 0.9 g/cm^3) to represent low-density polymers, and polyethylene terephthalate (PET; 1.4 g/cm^3) and polyester (PES; density:1.4 g/cm^3) to represent high-density polymers. PE, PES, and PET are among the most commonly produced polymers (PlasticsEurope, 2020). The pellets were purchased from a plastic manufacturer (Acordis). Fragments were obtained by cryo-crushing the pellets. Films were obtained by cutting pieces of packing films and plastic bottles. Fibers were obtained by cutting the bobbin threads. The added MPs could easily be distinguished from other particles (Fig. A.1) already present in the samples (contamination). Each pristine MP type was previously identified by Fourier transform infrared spectroscopy-attenuated total reflectance (FTIR-ATR) spectroscopy to check its polymeric composition (Constant et al., 2021b; see method details in Appendix A.).

Calibrated natural siliceous sand sediments (data from the manufacturer: >98% silica with a density of 2.65±0.05; SNL) were used in the experiments. The features and granulometry are presented in Appendix A (Table A.1 and Fig. A.2). Sediment and MPs were dried at 40 °C overnight and sieved using a sieve column (2, 1.25 mm; 800, 630, 500, 400, 315, 250, 200, 125, 80, and 40 µm) placed in a mechanical shaker. Sediment and MP size classes corresponded to the size classes obtained by sieving, except for fibers, which were measured when cut.

Table 1. Main features of the virgin MPs spiked in sediment matrices. LD: low-density; HD: high-density.

Polymer	**PE**			**PET**			**PES**
Shape (dimension)	Pellet (3D)	Fragment (3D)	Film (2D)	Pellet (3D)	Fragment (3D)	Film (2D)	Fiber (1D)
Density (g/cm^3)	0.9 (low-density)			1.4 (high-density)			
Type	LD Fragment/Pellet		LD Film	HD Fragment/Pellet		HD Film	HD Fiber
Size classe (mm)	3-4	1-2 0.5-0.63	3-4 1-2 0.5-0.63	3-4	1-2 0.5-0.63	3-4 1-2 0.5-0.63	3-4 1-2

2.1.2. Experimental setup

For all tests, approximately 350 g of dry sediment (corresponding to a height of approximately 8 cm of dry sediment in the column) was transferred to a plastic column with a height and length of 1 m and 6 cm, respectively (Fig. A.3). A total of 140 MPs (10 per size and type) were added to the top of the sediment layer. The top of the column was then filled with tap water (~10 L). The column was turned upside-down six times (we observed, during preliminary tests, that sediment did not sink homogeneously until 3-4 upside-down and we selected 6 reversals to keep a margin), with a sedimentation period of 10 min. After the sixth reversal and complete sedimentation of the particles (2 h), the floating particles were collected using a pipette with a large opening. Water was siphoned off and filtered through a 40-µm metal sieve. Particles collected on the sieve were pooled with those collected at the water surface and designated in the following text, figures, and tables as “floating MPs”. The sediments were pushed toward the upper part of the column, and five sections were cut with a metal trowel using a cylindrical guide and transferred to an aluminum container. The first section had a height of 0.5 cm (“surface” layer) and contained the MPs deposited on the sediment. The sediment was cut every 2 cm. The resulting five sediment sections and floating particles were dried at 40 °C overnight and then sieved through the same set of 12 sieves asused for sediment and MP preparation. The contents of the sieves were transferred to glass petri dishes. The experiment was repeated three times with 11 sediment size classes from 0.04 to 2 mm (i.e., 33 tests; Table A.1).

2.1.3. MP separation and counting

For most sieve contents, the amount of sediment was low, and MPs could directly be observed on petri dishes under a stereomicroscope. When the amount of sediment covered the MPs (> 5 g) and made the observation too laborious, the MPs were separated from the sediment using density-based NaI (1.6 g/mL) extraction according to Constant et al. (2021a, 2021b). In particular, the sediments were transferred to a glass container, and depending on the amount of sediment, 100-150 mL of extracting solution was added. After 30 s of manual agitation, the first centrifugation was conducted (5 min, 500 rpm), and the resulting supernatant was filtered through a metal sieve (40 µm). This extraction procedure (centrifugation and sieving) was repeated thrice. The collected materials were filtered through filter papers (Whatman©; 47 mm diameter; porosity of 2 µm). Finally, the filters and petri dishes were observed under a Leica MZ12 dissecting stereomicroscope (magnifications of 6 ×, 12 ×, and 25 ×). For all MP types, more than 90% of spiked MPs were recovered.

2.2. Estimation of vertical velocities and deposition: theoretical distribution

The vertical velocities (w_s) of the seven types of MPs (Table 1) were estimated based on two empirical equations (Equations 1 and 3). To infer the deposition pattern of the MPs in relation to the sediments in the absence of lateral transport (i.e., simple sedimentation), the vertical velocities of sediments were also calculated for two contrasting density intervals: between 1.5 and 1.7 (“soil”), representing clays, soils, or river sediments with a high organic matter content, and between 2.5 and 2.7 (“sand”), representing inorganic sediments.

Pellets and sediments were assimilated to spheres, whereas fragments and films were assimilated to flat pieces of variable proportions. The formula published by Zhiyao et al. (2008) was used for these shapes (Equation 1):

$$w_s = \frac{v}{d} d_*^3 [38.1 + 0.93\ d_*^{12/7}]^{-7/8} \quad (1)$$

where d_* is the dimensionless particle diameter (Equation 2), d is the diameter (mm), and v is the kinematic viscosity of the fluid ($mm^2.s^{-1}$). For fragments, d corresponds to a characteristic size equal to the cube root of the longest axis multiplied by the intermediate axis and the shortest axis.

$$d_* = \left(\frac{1}{v^2}\frac{g\left(\rho_w - \rho_p\right)}{\rho_w}\right)^{1/3} d \quad (2)$$

where g is the gravitational acceleration ($mm.s^{-2}$), ρ_p is the particle density, and ρ_w is the fluid density ($kg.m^{-3}$).

For fibers, we used the semi-empirical formula (Equation 3) published by Khatmullina and Isachenko (2017):

$$w_s = \frac{\pi}{2}\frac{1}{v}\frac{g\left(\rho_w - \rho_p\right)}{\rho_w}\frac{D\ L}{c1\ L + c2} \quad (3)$$

where D is the diameter (mm), L is the characteristic length (mm), ρ_p is the particle density ($kg.m^{-3}$), and $c1$ (mm^{-1}) and $c2$ (unit-less) are empirical coefficients.

For each type of particle, 10,000 estimations of w_s were calculated. The sizes of the particles were randomly retrieved over the size intervals used in the column experiment (MPs: 0.5-4 mm; sediments: 0.04-2 mm). Each size was associated with a density, which was also randomly retrieved over the density intervals of the polymers (Table 1) and the density intervals of the two contrasting sediments selected for deposit pattern comparison. Additional details regarding the used parameters are presented in Appendix A. (Table A.2).

w_s values were then partitioned by MP and sediment size classes (Tables 1, A.1, and A.2). For each class, the 2.5% ($Q_{0.025}$) and 97.5% ($Q_{0.975}$) quantiles, representing 95% of the particles, were selected to describe the vertical velocities. The resulting vertical velocity ranges ($Q_{0.025}$-$Q_{0.975}$) of MPs were then compared with those of the sediment. The deposition patterns were inferred by considering three situations (Fig. A.4):

- $w_{s[MP]} > w_{s[sediment]}$: MPs sink slower than sediments and settle at the top (surface) of the deposit.
- $w_{s[MP]} < w_{s[sediment]}$: MP sink faster than sediments and settle at the base (bottom) of the deposit.
- $w_{s[MP]} = w_{s[sediment]}$: MP sink as fast as the sediments and settle homogeneously between the top and bottom of the deposit (middle).

2.3. Data analysis

The percentage of MPs (%) was calculated for each pristine MP based on the number of MPs recovered within each sediment section compared to the total number of MPs recovered in all sections. Statistical analyses were conducted using R software (R Core Team, 2018), including the data manipulation packages "dplyr" (Wickham et al., 2017), "tidyr" (Wickham, 2021) and "purrr" (Henry and Wickham, 2020), and graphical package "ggpubr" (Kassambara, 2017) and colorblind-friendly color scale "viridis" (Garnier et al., 2021). As the normality of distribution was not observed (Shapiro-Wilk test), four non-parametric tests were conducted: the Wilcoxon-Man-Whitney test to compare two groups; Kruskal-Wallis test to compare more than two groups; Scheirer-Ray-Hare test to investigate the influence of two different factors and the interaction among factors; and post-hoc Dunn's test to compare the differences of all possible pairs and pinpoint specific medians that are significantly different from the others.

3. Results

3.1. Observed distribution from the column experiments

3.1.1. Floating MPs

Low-density MPs were significantly more abundant (62 ± 29%) within the water column than high-density polymers (7 ± 10%) (Wilcoxon-Man-Whitney test, $p < 0.01$; Table A.3).

The percentages of floating low-density polymers were very heterogeneous between tests, ranging from 29 to 87% (Fig. 1). The percentage of fragments/pellets was significantly higher (80 ± 20%) than those of films (46 ± 30%) (Wilcoxon-Man-Whitney test, $p < 0.01$). The percentages were not significantly different between each size class (Kruskal-Wallis test, $p = 0.80$). The interaction between the shape and size was not significant (SHR test, $p = 0.93$).

The percentages of floating high-density polymers varied moderately between tests, ranging from 0 to 33%. Fibers were significantly more abundant within the water column (11 ± 12%) than films and fragments/pellets (Wilcoxon-Man-Whitney test, $p < 0.01$). The percentages of fragments/pellets (5 ± 9%) and films did not differ significantly (Wilcoxon–Mann–Whitney test, $p = 0.89$). The percentages of floating MPs were not significantly different between each size class of fiber (Wilcoxon–Mann–Whitney test, $p = 0.23$). The percentages of small (0.5 mm) films and fragments/pellets (8 ± 10 and 11 ± 12%, respectively) were significantly higher than those of larger ones (1 and 4 mm) (3 ± 8 and 2 ± 5%, respectively) (Kruskal-Wallis test, $p < 0.01$). The interaction between the shape and size was not significant ($p = 0.31$).

PE fragments/pellets, PES fibers, and PET films were significantly less abundant within the water column with very fine sand (and fine sand for PE fragments/pellets) than with coarser sediments (Kruskal-Wallis test, $p < 0.01$, $p < 0.01$, and $p = 0.04$, respectively). The distribution of PE films and PET fragments/pellets was not significantly different across the sediment size classes (Kruskal-Wallis test, $p = 0.32$ and $p = 0.08$, respectively).

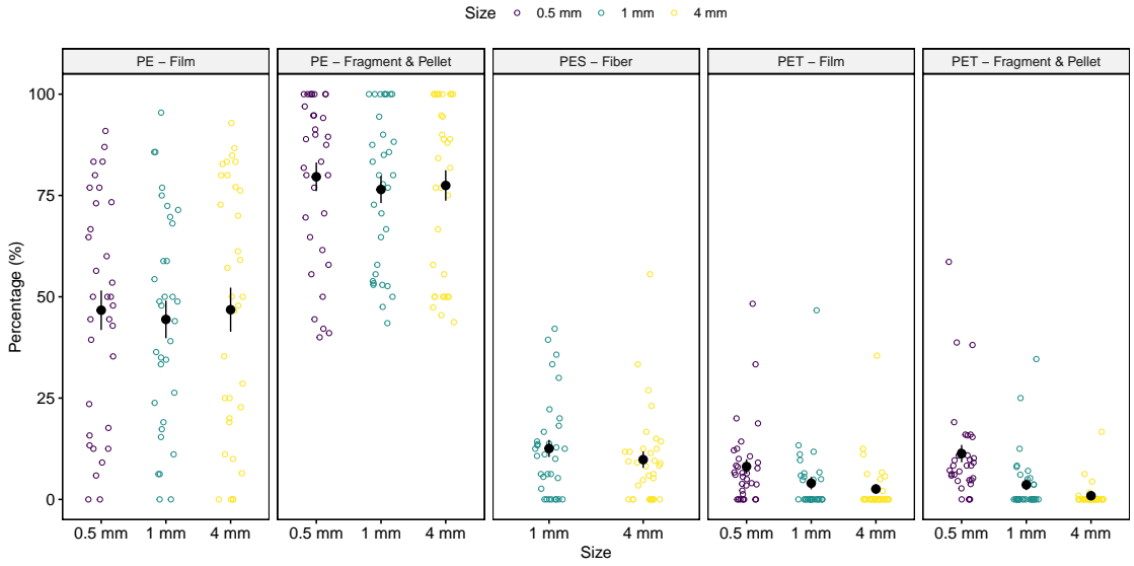

Fig. 1. Percentage of floating MPs (%) for each size, polymer, and shape. Small empty circles show the results of each test (i.e., 11 sediments × 3 replicates). Large solid circles and bars represent means and standard deviations, respectively.

3.1.2. Sinking MPs

The percentages of sinking low-density polymers were very heterogeneous between tests, ranging from 12 to 71% (Fig. 2). Within the sediment column, the distribution of low-density polymers changed between the films and fragments/pellets (Fig. 2). PE films were more heterogeneously distributed and mostly present at the surface of all sediment size classes, except for the finest sediment (40-80 µm), which was an important part of the bottom sediment column. PE fragments/pellets were homogeneously distributed along the vertical axis, with low percentages for each section, except for the finest sediment (40-80 µm), where most of them were present at the surface of the sediment column. The distributions were relatively similar between the sizes for both the film and fragments/pellets.

The percentages of sinking high-density polymers varied moderately between tests, ranging from 67 to 100% (Fig. 2). Inside the sediment column, the distribution changed with the sediment size class. At the smallest sediment size classes (40-80 µm), the majority of high-density MPs were concentrated in the bottom part of the sediment column. For larger sediment sizes, the MPs were less deeply distributed. In the largest size classes (> 630 µm), most of the high-density MPs were concentrated at the surface of the sediment column. The maximum concentrations of fibers were less deep than

those of fragments/pellets and films, except for the largest size classes (> 630 µm). Film and fragments/pellets had a relatively similar distribution. Fine and medium sand (125-500 µm) exhibited a unimodal distribution, skewed toward the bottom with fine sediments and toward the top with coarser sediment. Smallest fibers were deposited slightly deeper than larger ones (except at 40-80 µm), contrary to films and fragments/pellets, whose distributions became deeper with the increase in their sizes.

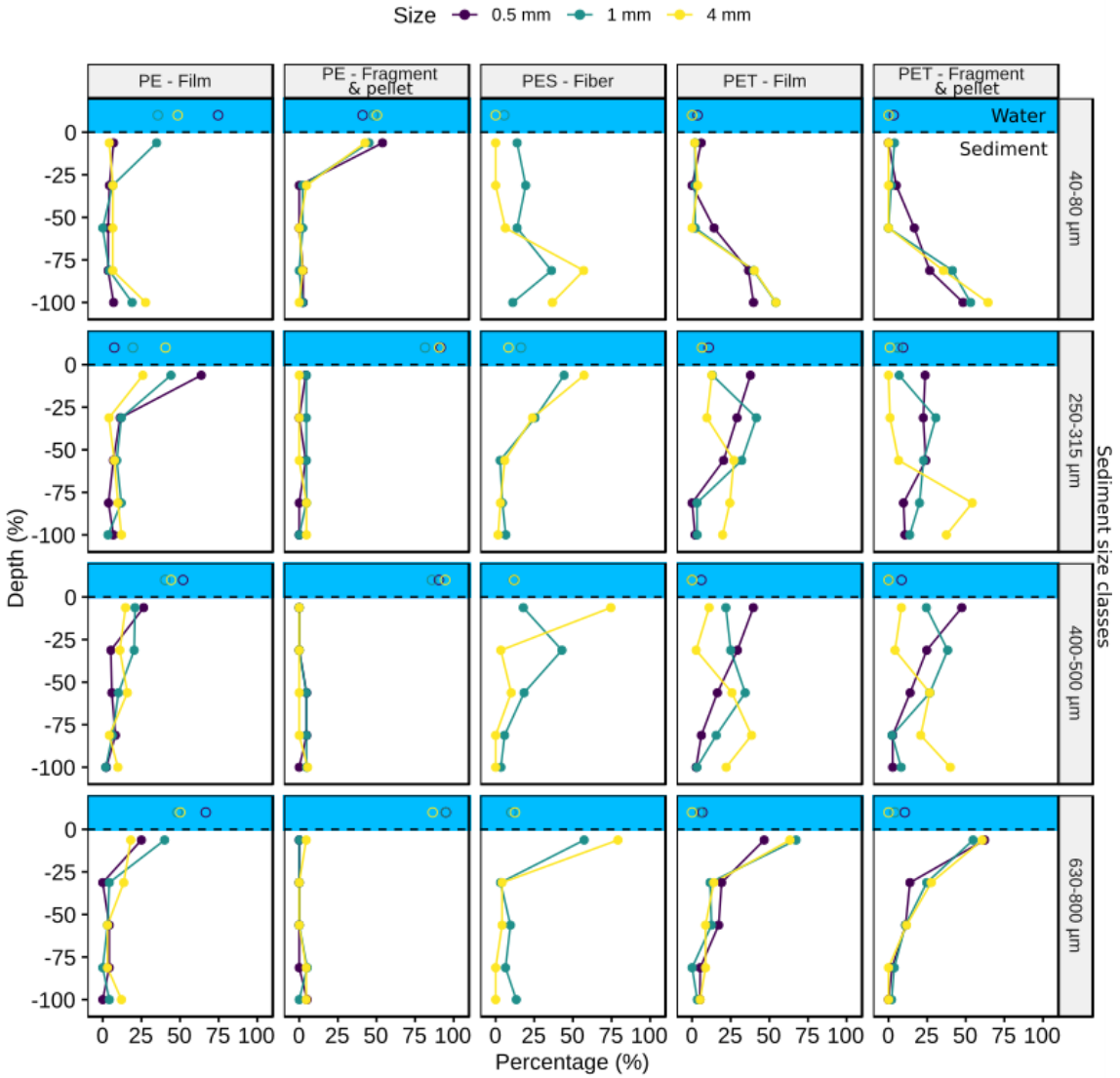

Fig. 2. Mean percentage (averages of three replicates) of MPs (%) within the water column and each sediment depth depending on four sediment grain size classes and sorting based on the polymer and shape. Empty circles represent the results within the water column (blue rectangle), whereas solid circles and lines represent the results within the sediment column. Fragment & pellet (PE and PET): 0.5 and 1 mm represent fragments, and 4 mm represent pellets. These four sediment size classes were selected because they show clearly visible changes from one to another. However, the entire set of results is displayed in Fig. A.5.

3.2. Theoretical distribution based on the simulated vertical velocity

The vertical velocities (w_s) were estimated (Table A.4) and compared for MPs and sediment particles over the size intervals of the column experiment (Figs. 3, A.6, and A.7). Low- and high-density polymers have a positive (rising) and negative (sinking) w_s values, respectively.

w_s values of the low-density polymers increase from smaller to larger particles and range between 0 and 0.05 m/s. Low-density films and fragments/pellets have similar w_s, excepted for those with a size of 0.5 mm, wherein the w_s values of fragments/pellets are slightly more positive.

High-density films and fragments/pellets show more negative w_s than fibers, excepted for films with a size of 0.5 mm. The w_s values of the fibers are roughly the same regardless of size, with a low negative vertical velocity ranging between 0 and -0.05 m/s. For films and fragments/ pellets, the w_s values decrease from smaller to larger and range from 0 to -0.15 m/s. Fragments with a size of 0.5 mm had slightly more negative w_s than the films with a size of 0.5 mm, but both their w_s values were similar at sizes of 1 and 4 mm. $w_{s,fiber}$ was more negative than w_s of the finest sediment (40-80 µm) and less negative than that of the coarsest sediments (soil: 630-800 µm; sand >400 µm). The w_s values of films and fragments/pellets are more negative than those of fine sediments (soil: <315 µm; sand: 40-80 µm), and the w_s values of the largest particles (4 mm) are more negative than those of the coarsest sediments (630-800 µm).

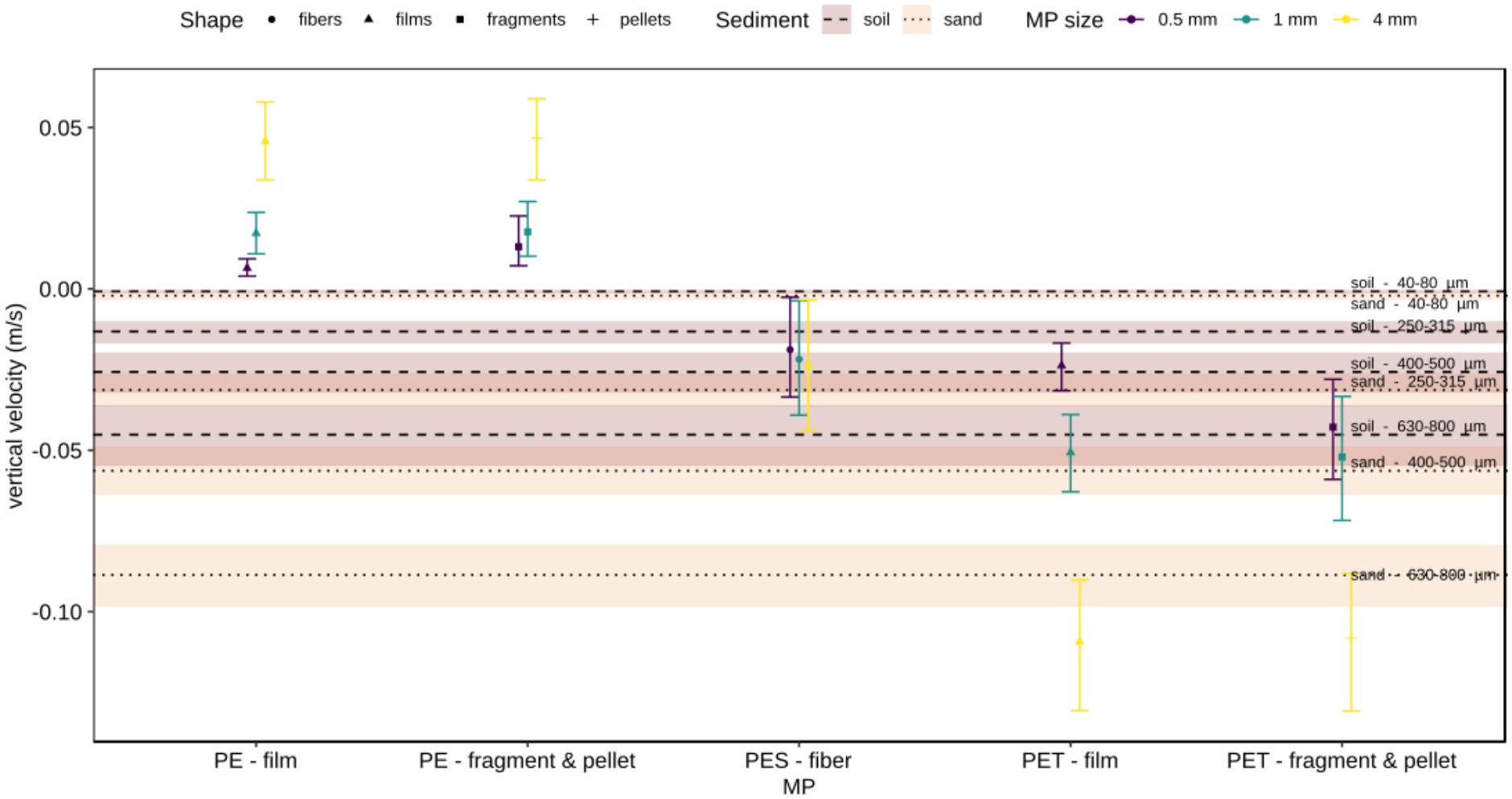

Fig. 3. Theoretical vertical velocities (m/s) of MPs and four sediment size classes. Icons and bars represent the means and interquartile ranges (95%) of the vertical velocity of MPs, respectively. Horizontal dashed lines and rectangles represent the means and interquartile ranges (95%) of the vertical velocity of soil (density: 1.5-1.7) and sand (density: 2.5-2.7), respectively. Fragments and pellets (PE and PET): 0.5 and 1 mm represent fragments (square) and 4 mm represent pellets (cross). Results for the 11 sediment size classes are shown in Fig. A.7. The details of the vertical velocity estimation in presented in section 2.2.

3.3. Comparison between the experiment and theory

We summarized the results acquired from the column experiments ("observed" distribution; Fig. 2) over three simplified depths (surface: top 0-0.5 cm; middle: between 0.5-6.5 cm; bottom: bottom 6.5-8 cm), and compared them with the expected deposition patterns ("theoretical" distribution) obtained using the vertical velocity results based on the hypothesis of simple sedimentation (Fig. 3; see method details in section 2.2). The observed distribution using sand was closer to the theoretical distribution estimated (density: 2.5-2.7) than that using with soil (density: 1.5-1.7) (Fig. 4 and A.9). To a large extent, the theoretical distribution of high-density MPs within soil is deeper than the observed distribution. Within the finest sediment size class (40-80 µm), high-density MPs should theoretically be below the sediment ("2.5" distribution). In the experiment ("observed" distribution), most of the MPs (60-80%) were expected to be effectively within the bottom section, but a significant portion of MPs (20-40%) were present in the middle part. PES fibers with a size of 1 mm were mainly (40-60%) present in the middle part. For the coarser sediments, the fiber-observed distributions are fairly similar to the 2.5-density theoretical distributions, slightly below the distributions of particles with sizes of 400-500 µm and 600-830 µm. For the 250-315 µm fraction, the PET was mainly above the theoretical distribution. For the 400-500 µm fraction, the observed distribution was similar to the theoretical distribution for the films with a size of 1 mm and fragments with a size of 0.5 mm, and slightly above the theoretical distribution for the other films and fragments/pellets. Finally, for the largest sediment size class (600-830 µm), high-density MPs were mainly present at the surface, whereas simulated vertical velocities predicted a deeper distribution for large films and fragments/pellets (4 mm).

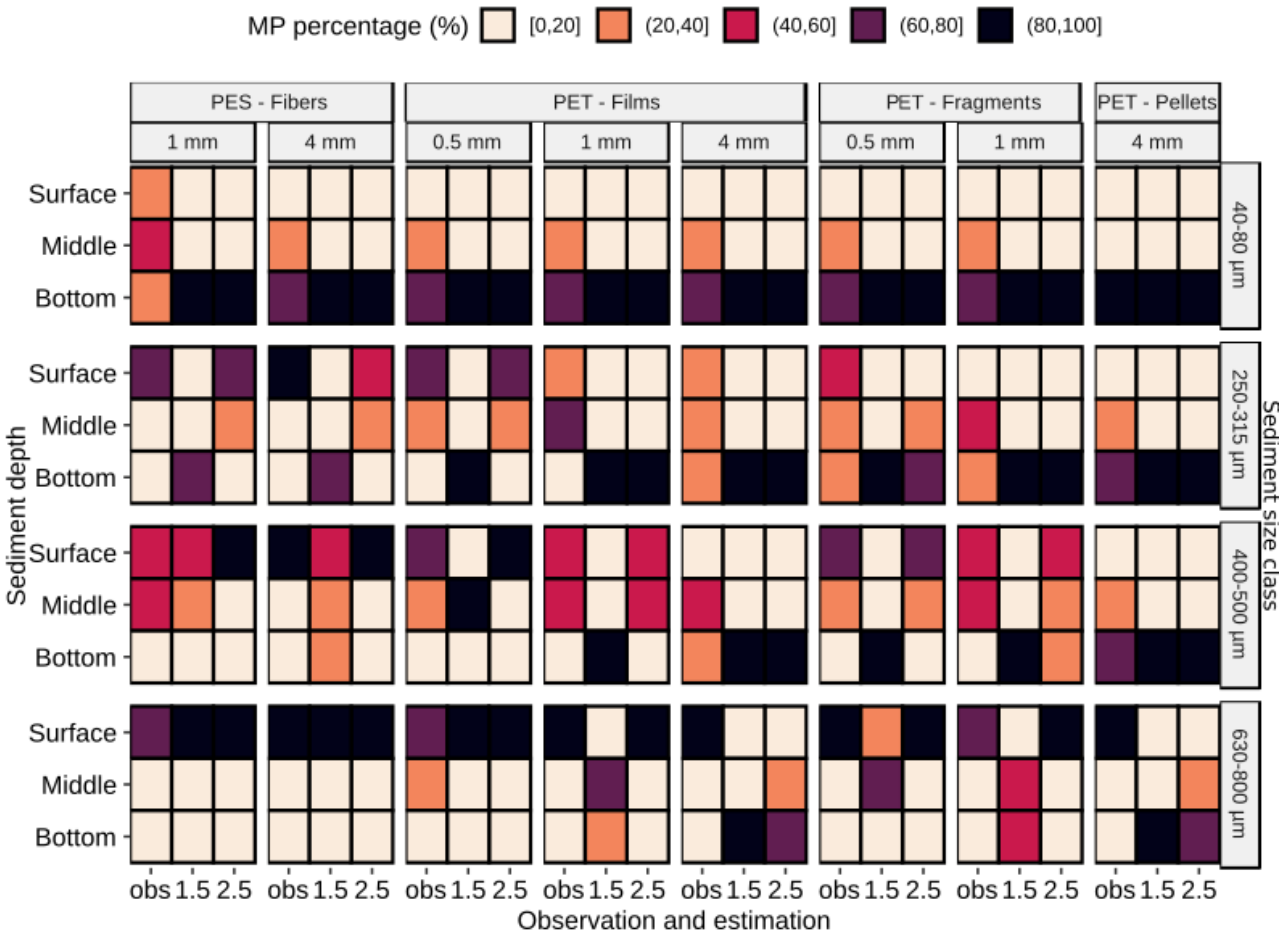

Fig. 4. Observed and theoretical distributions of high-density polymers (PES and PET) within three simplified sediment depths (surface, middle, and bottom) depending on four sediment size classes sorted according to the polymer and shape. Observed (obs) MP percentages are the average of three replicates. Observation and estimation: "observed distribution" (obs), theoretical distribution with soil of "density 1.5-1.7" (1.5), and sand of "density 2.5-2.7" (2.5). Details about the theoretical distributions are presented in section 2.2. Sediment depth: "top 0-0.5 cm" (surface), "between 0.5-6.5 cm" (middle), "bottom 6.5-8 cm" (bottom). Low-density polymers (PE) have a positive vertical velocity and are theoretically not present within the sediment. Results for the 11 sediment size classes are shown in Fig. A.8. Differences between the observation and estimation are shown in Figs. A.9 and A.10.

4. Discussion

Theoretically, two major processes occur after the resuspension of the sediment: the settling or the rise of the particles in the water column, followed by the superposition of the sinking particles on top of each other (Baba and Komar, 1981). In the water column, the movement of particles also depends on their properties and interactions with each other (Kooi et al., 2018). Denser, larger, and more spherical particles settle faster; however, some processes (e.g., particle aggregation) can modify this pattern (Alimi et al., 2017; Andersen et al., 2021; Leiser et al., 2021; Li et al., 2022, 2019). The superposition pattern of the particles is related to their settling velocity, as well as their capacity to slip into the interstices between other particles during deposition (infiltration behavior). In this experiment, infiltration was presumed to be negligible, as the large size of the MPs drastically reduced the probability of infiltration (Waldschläger and Schüttrumpf, 2020).

In the column experiments, the distribution of MPs varied greatly within and among the sediments. The MP type also plays a key role in this distribution. Nevertheless, some patterns were clearly demonstrated. The features of the sediment (density and size) and MPs (density, size, and shape) influence the deposition of MPs, but to different degrees. Additionally, the characteristics interact with each other, resulting in opposing trends. We observed that the distribution of MPs was directly related to their density, wherein the majority of low-density polymers remained in the water column after resuspension, whereas the majority of high-density polymers were trapped in the bulk sediment (i.e., throughout the sediment column). The vertical distribution of MPs within the sediment also changes with sediment features. Overall, the percentage of MPs reaching the deepest sections increased with decreasing sediment grain size. The vertical distribution of high-density polymers also changes according to their shape. Fibers were found to be more abundant than pellets, fragments, and films. Finally, the distributions of fragments/pellets and films changes with their sizes, in contrast to that of fibers. Thus, with the sediments tested, the distribution of MPs was roughly consistent with their theoretical order of sinking and appeared to be preliminarily related to their settling velocities.

The most important deviation from theory is the significant fraction of low-density polymer that settle at the top of the sediment (Fig. 1). Low-density polymers have positive vertical velocities, which force them to rise within the water column. Particle adhesion, aggregation, or biofouling may decrease the vertical velocity of low-density polymers (Chubarenko et al., 2016; Leiser et al., 2021). According to the used equations, the rising velocities of the PE change with size but not with shape (Fig. 3). However, the observed distribution of low-density MPs is affected by the particle shape, as mentioned by Waldschläger et al. (2020), they observed that the rising velocity of films was lower than that of fragments and highlighted the deformation behavior of films. For the same size and density, the irregular shape of a particle, compared to a sphere, increases its secondary movements (i.e., not vertical), which retards its sinking or rising behavior (Waldschläger and Schüttrumpf, 2019a). Additionally, films might be particularly sensitive to particle adhesion, aggregation, or biofouling (in nature but not in these experiments) because of their high surface-area-to-volume ratio (Chubarenko et al., 2016). High-density polymers also constitute a small but significant fraction that reaches the water column. Moreover, for low-density polymers, interactions with "slower" particles (e.g., fine sediments or organic matters) may decrease the settling velocity of particles (Chubarenko et al., 2016). However, this result has an important probability of being an artifact. Notably, virgin MPs can have a significant hydrophobicity ((Al Harraq et al., 2022); more details are presented in the last paragraph of the discussion). To a lesser extent, the distribution of high-density fibers in the sediment also deviates from expectations. Theoretically, the influence of the fiber size is low. Notably, fibers align and sink horizontally at the same velocity, regardless of their length (Waldschläger and Schüttrumpf, 2019a). Moreover, thinner fibers can infiltrate deeper (Waldschläger and Schüttrumpf, 2020), but the fibers used in the experiment had the same diameter, and as mentioned above, such phenomena have a low probability of occurrence. In the experiment, small fibers tended to be deposited slightly deeper in fine and coarse sediment than in large fibers, and the opposite was true in very fine sediment (namely, large fibers were deposited above small fibers). As the fibers are regular cylinders, the surface of the contact increases with the length (at a constant diameter), which

may explain the slight difference observed in our study. Finally, the sedimentation of low-density MPs increases with very fine sediments for fragments/ pellets, but not for films. Li et al. (2022) observed that the settling rate of small polystyrene microspheres (<300 μm) increased in fine suspended sediment (median: 16.3 μm) compared to that in no sediment.

Xia et al. (2021) studied the resuspension of MPs within columns of sediment samples using a customized particle entrapment simulator (PES) device. Compared to that in the control samples (i.e., undisturbed), a higher proportion of small-sized MPs (50–500 μm) was observed within the overlying water or the deep sediment and a lower proportion settled at the sediment surface, suggesting a disturbance-induced transport from the sediment surface. No change was observed in the distribution of large-sized MPs (0.5-5 mm). Unfortunately, their results cannot be compared with those in our study, as the authors did not indicate whether density and shape affected these patterns.

Overall, the observed distribution of virgin MPs was in accordance with the expected distribution based on the vertical velocity formulas (Fig. 4). The formulas logically did not predict the sedimentation of low-density polymers but tended to position high-density polymers lower in the sediment. Excluding the potential biases of the experiment (see details below), these results may be explained either by a misconfiguration of some parameters in the formulas or by the absence of parameters on the effect of particle interactions. The vertical velocity formulas used here are based on Stokes' formula and include empirical parameters determined in previous experimental studies (section 2.2). These parameters should be corrected in further experiments considering the high diversity of MPs (Kooi et al., 2018). Some equations accounting for microbial colonization have been proposed (Nguyen et al., 2020), but parameters accounting for hetero-aggregation with inorganic particles are still missing (Alimi et al., 2017). This study highlights the importance of including the latter in future theoretical studies. Finally, the vertical velocity formulas can be used in the first approximation, but still need to be strengthened.

Before presenting some assumptions regarding the environmental implications of these observations, it is necessary to mention the limitations of this experiment. First, MPs were placed at the surface of the sediment, which may have induced different results than if the MPs and sediment particles were mixed in advance. However, as column reversal was conducted six times, this bias was probably limited. Second, the experiments displayed a simplified version of the conditions occurring in natural systems. In natural environments, sediment movements are not horizontally restricted, and flow velocity is rarely null; therefore, sedimentation is probably more diffuse. This may also result in an amplified trapping effect due to a high concentration of particles, which transport some MPs in the sedimentary flux independently of their sedimentation behavior. In contrast, the column may engender the wall effect (Baba and Komar, 1981) and generate air bubbles (Waldschläger and Schüttrumpf, 2019a), both of which may modify the settling or rising velocity. Finally, we used virgin MPs to increase the repeatability of the experiments and facilitate the counting procedure; however, they are more prone to have a significant hydrophobicity (Al Harraq et al., 2022)) and are not associated with other solids, such as biofilms, for a long time. In addition, composition and surface coating may influence the interaction with other particles, including homo- and hetero-aggregation (Wang et al., 2021). Considering these limitations, some hypotheses on the fate of MPs are proposed: (i) the physical perturbation of the sediment may modify the distribution and pool of MPs; (ii) low-density polymers trapped in the sediment may be released to the water column and be dragged along by the current; (iii) they may settle subsequently, especially films, but will be concentrated at the surface of the sediments; (iv) high-density polymers have a higher probability of being trapped again in the sediment, and their global vertical distribution will depend on the sediment grain size, but also on the nature of the MPs themselves (size and shape). This last point explains, in to a certain extent, why no relevant correlation has been observed between sediment grain size and MP distribution in field studies (Constant et al., 2021a; Corcoran et al., 2020; Vermaire et al., 2017).

All these hypotheses examine the consequences of sediment resuspension in aquatic systems, where lateral transfers (currents) are limited (lakes and canalized rivers in particular). This may cause

bioturbation phenomena at a scale of millimeters or centimeters, wave action at scales of several centimeters or even tens of centimeters when propellers touch the sediment surface, and dredging at scales of several tens of centimeters to a meter because these processes systematically lead to important sediment remobilization.

5. Conclusion

This study investigated key parameters to understand the sdeposition and sinking of MPs by experimentally and theoretically comparing the distributions of MPs in water and sediment after the remobilization of sediments without lateral transport (i.e., low-velocity flow). Fourteen combinations of density, size, and shape of MPs were tested for light and dense pristine polymers in 11 sediment grain sizes. The main conclusions based on the 33 experimental tests and simple sedimentation simulations are as follows:

(1) The observed distribution largely follows the deposition pattern induced by differential vertical velocities between particles: most the low-density polymers float; most the high-density polymers settle deeper in fine sediments than in coarse ones; high-density pellets, fragments, and films settle deeper than fibers and pellet, and large fragments and films settle deeper than small ones.

(2) Unexpectedly, an important part of the low-density polymers settled at the surface of the sediment. This pattern was more important for films than fragments and pellets, probably because of the specific vertical behavior of the films. The sedimentation of low-density fragments increased with very fine sediments, thereby highlighting the importance of particle interactions. The effect of shape was not the same for high- and low-density polymers.

(3) Vertical velocity formulas roughly predict the distribution of MPs but tend to position high-density polymers lower in fine sediment and upper in coarse sediment. Vertical velocity formulas could therefore be useful as a preliminary approach but still need to be improved.

This study can be regarded as a first step in the investigation of MP deposition in disturbed sediments, as many questions still need to be answered. Further experiments should be conducted on the effects of organic matter and heterogeneous-sized sediments, as well as the effects of the MP degradation state and their associations with other particles, such as biofilms, on the MP deposition behavior. Finally, from the initial conclusions of vertical particle sedimentation, interesting results can be

obtained by integrating the lateral transport of particles during the experiments and theoretical models, as is the case in rivers, estuaries, and seawater.

CRedit authorship contribution statement

Mel Constant: Methodology, Investigation, Writing - Original Draft. Claire Alary: Conceptualization, Writing - Review & Editing, Supervision. Lisa Weiss: Formal analysis, Writing - Review & Editing. Alix Constant: Investigation. Gabriel Billon: Conceptualization, Writing - Review & Editing, Supervision.

Declaration of competing interest

The authors declare that they have no known competing financial interests or personal relationships that could have appeared to influence the work reported in this paper.

Acknowledgements

We acknowledge the European Fund for Regional Development Interreg for funding the post-doc grant of Mel Constant and the internship of Alix Constant, and supported this research through the VALSE project. We thank LGCgE lab members Johanna Caboche, Guillaume Potier, Damien Betrancourt and Dominique Dubois for their helps with laboratory work, Vincent Thiery for his advises on the use of the dissecting stereo-microscope, and Laurent Charlet to furnishing and crushing plastic pellets.

Appendix A. Supplementary data

Methods: spectroscopy FTIR.

Figures: Photos of MPs spiked (A.1) and the column (A.3), grain size distribution (A.2), explanatory diagram of section 2.2 (A.4), percentage of floating MPs (A.5), theoretical vertical velocities (A.6 and A.7), observed and theoretical distributions (A.8), and difference between them (A.9 and A.10).

Tables: Grain size distribution (A.1), parameters and results of w_s (A.2 and A.4), and statistical analysis (A.3).

References

Al Harraq, A., Brahana, P.J., Arcemont, O., Zhang, D., Valsaraj, K.T., Bharti, B., 2022. Effects of Weathering on Microplastic Dispersibility and Pollutant Uptake Capacity. ACS Environ. Au 2, 549–555. https://doi.org/10.1021/acsenvironau.2c00036

Alimi, O., Farner Budarz, J., Hernandez, L.M., Tufenkji, N., 2017. Microplastics and Nanoplastics in Aquatic Environments: Aggregation, Deposition, and Enhanced Contaminant Transport. Environ. Sci. Technol. https://doi.org/10.1021/acs.est.7b05559

Allen, S., Allen, D., Phoenix, V.R., Le Roux, G., Durántez Jiménez, P., Simonneau, A., Binet, S., Galop, D., 2019. Atmospheric transport and deposition of microplastics in a remote mountain catchment. Nat. Geosci. 12, 339–344. https://doi.org/10.1038/s41561-019-0335-5

Andersen, T.J., Rominikan, S., Olsen, I.S., Skinnebach, K.H., Fruergaard, M., 2021. Flocculation of PVC Microplastic and Fine-Grained Cohesive Sediment at Environmentally Realistic Concentrations. The Biological Bulletin 240, 42–51. https://doi.org/10.1086/712929

Andrady, A.L., 2015. Persistence of Plastic Litter in the Oceans, in: Bergmann, M., Gutow, L., Klages, M. (Eds.), Marine Anthropogenic Litter. Springer International Publishing, pp. 57–72. https://doi.org/10.1007/978-3-319-16510-3_3

Baba, J., Komar, P.D., 1981. Measurements and analysis of setting velocities of natural quartz sand grains. Journal of Sedimentary Research 51, 631–640. https://doi.org/10.2110/jsr.51.631

Baldock, T.E., Tomkins, M.R., Nielsen, P., Hughes, M.G., 2004. Settling velocity of sediments at high concentrations. Coastal Engineering 51, 91–100. https://doi.org/10.1016/j.coastaleng.2003.12.004

Chubarenko, I., Bagaev, A., Zobkov, M., Esiukova, E., 2016. On some physical and dynamical properties of microplastic particles in marine environment. Marine Pollution Bulletin 108, 105–112. https://doi.org/10.1016/j.marpolbul.2016.04.048

Constant, M., Alary, C., De Waele, I., Dumoulin, D., Breton, N., Billon, G., 2021a. To What Extent Can Micro- and Macroplastics Be Trapped in Sedimentary Particles? A Case Study Investigating Dredged Sediments. Environ. Sci. Technol. 55, 5898–5905. https://doi.org/10.1021/acs.est.0c08386

Constant, M., Billon, G., Breton, N., Alary, C., 2021b. Extraction of microplastics from sediment matrices: Experimental comparative analysis. Journal of Hazardous Materials 420, 126571. https://doi.org/10.1016/j.jhazmat.2021.126571

Constant, M., Kerhervé, P., Heussner, S., 2017. Source, Transfer, and Fate of Microplastics in the Northwestern Mediterranean Sea: A Holistic Approach, in: Baztan, J., Jorgensen, B., Pahl, S., Thompson, R.C., Vanderlinden, J.-P. (Eds.), Fate and Impact of Microplastics in Marine Ecosystems. Elsevier, pp. 115–116. https://doi.org/10.1016/B978-0-12-812271-6.00111-3

Corcoran, P.L., Belontz, S.L., Ryan, K., Walzak, M.J., 2020. Factors Controlling the Distribution of Microplastic Particles in Benthic Sediment of the Thames River, Canada. Environ. Sci. Technol. 54, 818–825. https://doi.org/10.1021/acs.est.9b04896

Dhivert, E., Phuong, N.N., Mourier, B., Grosbois, C., Gasperi, J., 2022. Microplastic trapping in dam reservoirs driven by complex hydrosedimentary processes (Villerest Reservoir, Loire River, France). Water Res. 225, 119187. https://doi.org/10.1016/j.watres.2022.119187

Garnier, Simon, Ross, Noam, Rudis, Robert, Camargo, Pedro, A., Sciaini, Marco, Scherer, Cédric, 2021. viridis - Colorblind-Friendly Color Maps for R. https://doi.org/10.5281/zenodo.4679424

GESAMP, 2015. Sources, fate and effects of microplastics in the marine environment: a global assessment, IMO/FAO/UNESCO-IOC/UNIDO/WMO/IAEA/UN/UNEP/UNDP Joint Group of Experts on the Scientific Aspects of Marine Environmental Protection). ed, Rep. Stud. GESAMP. https://doi.org/10.13140/RG.2.1.3803.7925

He, D., Zhang, X., Hu, J., 2021. Methods for separating microplastics from complex solid matrices: Comparative analysis. Journal of Hazardous Materials 409, 124640. https://doi.org/10.1016/j.jhazmat.2020.124640

Henry, L., Wickham, H., 2020. purrr: Functional Programming Tools.

Horton, A.A., 2021. Plastic pollution: when do we know enough? Journal of Hazardous Materials 126885. https://doi.org/10.1016/j.jhazmat.2021.126885
Kassambara, A., 2017. Ggpubr: 'Ggplot2' based publication ready plots. https://doi.org/. https://CRAN.R-project.org/package=ggpubr
Khatmullina, L., Isachenko, I., 2017. Settling velocity of microplastic particles of regular shapes. Marine Pollution Bulletin 114, 871–880. https://doi.org/10.1016/j.marpolbul.2016.11.024
Kooi, M., Besseling, E., Kroeze, C., Wenzel, A.P. van, Koelmans, A.A., 2018. Modeling the Fate and Transport of Plastic Debris in Freshwaters: Review and Guidance, in: Freshwater Microplastics, The Handbook of Environmental Chemistry. Springer, Cham, pp. 125–152. https://doi.org/10.1007/978-3-319-61615-5_7
Lebreton, L., Andrady, A., 2019. Future scenarios of global plastic waste generation and disposal. Palgrave Commun 5, 1–11. https://doi.org/10.1057/s41599-018-0212-7
Leiser, R., Schumann, M., Dadi, T., Wendt-Potthoff, K., 2021. Burial of microplastics in freshwater sediments facilitated by iron-organo flocs. Sci Rep 11, 24072. https://doi.org/10.1038/s41598-021-02748-4
Li, W., Zu, B., Hu, L., Lan, L., Zhang, Y., Li, J., 2022. Migration behaviors of microplastics in sediment-bearing turbulence: Aggregation, settlement, and resuspension. Marine Pollution Bulletin 180, 113775. https://doi.org/10.1016/j.marpolbul.2022.113775
Li, Y., Wang, X., Fu, W., Xia, X., Liu, C., Min, J., Zhang, W., Crittenden, J.C., 2019. Interactions between nano/micro plastics and suspended sediment in water: Implications on aggregation and settling. Water Research 161, 486–495. https://doi.org/10.1016/j.watres.2019.06.018
Miller, R.Z., Watts, A.J.R., Winslow, B.O., Galloway, T.S., Barrows, A.P.W., 2017. Mountains to the sea: River study of plastic and non-plastic microfiber pollution in the northeast USA. Marine Pollution Bulletin 124, 245–251. https://doi.org/10.1016/j.marpolbul.2017.07.028
Nguyen, T.H., Tang, F.H.M., Maggi, F., 2020. Sinking of microbial-associated microplastics in natural waters. PLOS ONE 15, e0228209. https://doi.org/10.1371/journal.pone.0228209
Nizzetto, L., Bussi, G., Futter, M.N., Butterfield, D., Whitehead, P.G., 2016. A theoretical assessment of microplastic transport in river catchments and their retention by soils and river sediments. Environmental Science-Processes & Impacts 18, 1050–1059. https://doi.org/10.1039/c6em00206d
Petersen, F., Hubbart, J.A., 2021. The occurrence and transport of microplastics: The state of the science. Science of The Total Environment 758, 143936. https://doi.org/10.1016/j.scitotenv.2020.143936
PlasticsEurope, 2020. Plastics - The Facts 2020 - An analysis of European plastics production, demand and waste data.
R Core Team, 2018. R: A Language and Environment for Statistical Computing. R Foundation for Statistical Computing, Vienna, Austria. https://www.R-project.org/
Rochman, C.M., 2018. Microplastics research—from sink to source. Science 360, 28–29. https://doi.org/10.1126/science.aar7734
Rochman, C.M., 2015. The Complex Mixture, Fate and Toxicity of Chemicals Associated with Plastic Debris in the Marine Environment, in: Bergmann, M., Gutow, L., Klages, M. (Eds.), Marine Anthropogenic Litter. Springer International Publishing, Cham, pp. 117–140. https://doi.org/10.1007/978-3-319-16510-3_5
Rochman, C.M., Brookson, C., Bikker, J., Djuric, N., Earn, A., Bucci, K., Athey, S., Huntington, A., McIlwraith, H., Munno, K., De Frond, H., Kolomijeca, A., Erdle, L., Grbic, J., Bayoumi, M., Borrelle, S.B., Wu, T., Santoro, S., Werbowski, L.M., Zhu, X., Giles, R.K., Hamilton, B.M., Thaysen, C., Kaura, A., Klasios, N., Ead, L., Kim, J., Sherlock, C., Ho, A., Hung, C., 2019. Rethinking microplastics as a diverse contaminant suite. Environmental Toxicology and Chemistry 38, 703–711. https://doi.org/10.1002/etc.4371
Santos, R.G., Machovsky-Capuska, G.E., Andrades, R., 2021. Plastic ingestion as an evolutionary trap: Toward a holistic understanding. Science 373, 56–60. https://doi.org/10.1126/science.abh0945

UNEP and GRID-Arendal, 2016. Marine Litter Vital Graphics. https://doi.org/10.13140/RG.2.2.20593.89442

Vermaire, J.C., Pomeroy, C., Herczegh, S.M., Haggart, O., Murphy, M., 2017. Microplastic abundance and distribution in the open water and sediment of the Ottawa River, Canada, and its tributaries. Facets 2, 301–314. https://doi.org/10.1139/facets-2016-0070

Waldschläger, K., Born, M., Cowger, W., Gray, A., Schüttrumpf, H., 2020. Settling and rising velocities of environmentally weathered micro- and macroplastic particles. Environmental Research 191, 110192. https://doi.org/10.1016/j.envres.2020.110192

Waldschläger, K., Brückner, M.Z.M., Carney Almroth, B., Hackney, C.R., Adyel, T.M., Alimi, O.S., Belontz, S.L., Cowger, W., Doyle, D., Gray, A., Kane, I., Kooi, M., Kramer, M., Lechthaler, S., Michie, L., Nordam, T., Pohl, F., Russell, C., Thit, A., Umar, W., Valero, D., Varrani, A., Warrier, A.K., Woodall, L.C., Wu, N., 2022. Learning from natural sediments to tackle microplastics challenges: A multidisciplinary perspective. Earth-Science Reviews 228, 104021. https://doi.org/10.1016/j.earscirev.2022.104021

Waldschläger, K., Schüttrumpf, H., 2020. Infiltration Behavior of Microplastic Particles with Different Densities, Sizes, and Shapes—From Glass Spheres to Natural Sediments. Environ. Sci. Technol. 54, 9366–9373. https://doi.org/10.1021/acs.est.0c01722

Waldschläger, K., Schüttrumpf, H., 2019a. Effects of Particle Properties on the Settling and Rise Velocities of Microplastics in Freshwater under Laboratory Conditions. Environ. Sci. Technol. 53, 1958–1966. https://doi.org/10.1021/acs.est.8b06794

Waldschläger, K., Schüttrumpf, H., 2019b. Erosion Behavior of Different Microplastic Particles in Comparison to Natural Sediments. Environ. Sci. Technol. 53, 13219–13227. https://doi.org/10.1021/acs.est.9b05394

Wang, X., Bolan, N., Tsang, D.C.W., Sarkar, B., Bradney, L., Li, Y., 2021. A review of microplastics aggregation in aquatic environment: Influence factors, analytical methods, and environmental implications. Journal of Hazardous Materials 402, 123496. https://doi.org/10.1016/j.jhazmat.2020.123496

Weiss, L., Ludwig, W., Heussner, S., Canals, M., Ghiglione, J.-F., Estournel, C., Constant, M., Kerhervé, P., 2021. The missing ocean plastic sink: Gone with the rivers. Science 373, 107–111. https://doi.org/10.1126/science.abe0290

Wickham, H., 2021. tidyr: Tidy Messy Data.

Wickham, H., François, R., Henry, L., Müller, K., 2017. dplyr: a grammar of data manipulation. https://CRAN.R-project.org/package=dplyr

Xia, F., Yao, Q., Zhang, J., Wang, D., 2021. Effects of seasonal variation and resuspension on microplastics in river sediments. Environmental Pollution 117403. https://doi.org/10.1016/j.envpol.2021.117403

Yan, M., Wang, L., Dai, Y., Sun, H., Liu, C., 2021. Behavior of Microplastics in Inland Waters: Aggregation, Settlement, and Transport. Bull Environ Contam Toxicol 107, 700–709. https://doi.org/10.1007/s00128-020-03087-2

Zhang, Y., Pu, S., Lv, X., Gao, Y., Ge, L., 2020. Global trends and prospects in microplastics research: A bibliometric analysis. Journal of Hazardous Materials 400, 123110. https://doi.org/10.1016/j.jhazmat.2020.123110

Zhiyao, S., Tingting, W., Fumin, X., Ruijie, L., 2008. A simple formula for predicting settling velocity of sediment particles. Water Science and Engineering 1, 37–43. https://doi.org/10.1016/S1674-2370(15)30017-X